Korean J. Chem. Eng., 39(4), 928-933 (2022)
DOI: 10.1007/s11814-021-1019-6

pISSN: 0256-1115
eISSN: 1975-7220

Electrochemical performance of graphite/silicon/pitch anode composite prepared by metal etching process

Yoon Ji Jo, Na Hyun Choi, and Jong Dae Lee†

Department of Chemical Engineering, Chungbuk National University,
1, Chungdaero, Seowon-gu, Cheongju, Chungbuk 28644, Korea
(*Received 18 May 2021 • Revised 6 October 2021 • Accepted 17 November 2021*)

Abstract−The electrochemical characteristics of graphite/silicon/pitch composites were investigated as anode material in lithium ion batteries. The anode materials were prepared with etched graphite using nickel chloride hexahydrate. Scanning electron microscopy, x-ray diffraction and thermogravimetric analysis were used to analyze the physical properties of graphite/silicon/pitch composites. The electrochemical characteristics of the batteries were investigated by charge-discharge cycle, rate performance, cyclic voltammetry and electrochemical impedance spectroscopy tests in the eletrolyte of 1.0 M $LiPF_6$ (EC : DMC : DEC=1 : 1 : 1 vol%). Graphite/silicon/pitch electrode showed better electrochemical properties than the graphite electrode, and even nickel etched graphite was superior to graphite. Also, it was confirmed that both capacity and rate performance are significantly improved when the ratio of graphite, silicon, and pitch is 8 : 1 : 1 ($G_8Si_1P_1$). It is found that $G_8Si_1P_1$ has the initial discharge capacity of 680 mAh/g, the capacity retention ratio of 90% during 100 cycles and the retention rate capability of 91% in 2 C/0.1 C, 87% in 5 C/0.1 C.

Keywords: Etched Graphite, Silicon, Pitch, Anode Materials, Lithium Ion Batteries

INTRODUCTION

To solve the problem of global climate change caused by the use of fossil energy sources, studies have focused on lithium-ion battery (LIB) systems for electric vehicles, hybrid electric vehicles, and energy storage systems. However, the performance of conventional LIBs cannot satisfy the requirements of a high-performance power source, including high energy and power density, long cycle life, low cost, and stability. To meet the market demand for a longer lifecycle, lighter battery weight, and rapid charge rate, the energy density of LIBs should continuously be improved [1,2]. LIBs consist of a cathode, anode, a separator membrane, and electrolyte. Carbon-based materials are mainly used for the anode, and development of a high-capacity anode material that replaces commercial materials is required to improve performance.

Although graphite is the most widely used commercial anode material, the limited theoretical capacity (372 mAh/g) does not meet the energy density and performance required to satisfy the increasing energy demand [3]. For high charging currents, in particular, the phenomenon of large polarization in graphite anodes leads to the deposition of Li. The resulting Li deposit is electrically insulated and reacts with the electrolyte to increase the internal resistance and decrease the energy density of the battery. Graphite electrodes are generally known to undergo rapid capacity decline due to Li deposition [4]. To overcome this limitation, studies have long pursued the development of high-performance anode materials with high Li^+ storage capacity at low operating voltage [5].

Materials such as Si, Sn, and Ge have been suggested as substitutes for graphite, among which Si has a high theoretical capacity (4,200 mAh/g in the form of $Li_{22}Si_5$ at 145 °C and 3,590 $mAh \cdot g^{-1}$ in the form of $Li_{15}Si_4$ at room temperature), low discharge potential (~0.5 V versus Li/Li^+), and environmental friendliness, and is thus regarded as the most desirable alternative anode material [6]. However, the rapid variation in the volume (>300%), poor electrical conductivity (~10^{-4} S/m), and the formation of unstable solid electrolyte interphase (SEI) layer mean that Si has low cycle life due to structural degradation of the electrode and high charge transfer resistance [7]. One safety issue is the expansion of the Si electrode, which compresses the electrolyte and reduces Li^+ transfer [8]. Silicon composites containing a carbon-based material such as graphite or pitch can be an alternative to reduce volume expansion of silicon. Among carbon-based materials, petroleum pitch coating can improve cycle stability and electrical conductivity. Moreover, pitch coating forms a uniform protective film by reducing surface defects of composite materials and improves initial efficiency by suppressing unstable SEI layer formation [9].

A recent study reported the synergistic effect of graphite and silicon composites, which resulted in high energy density and reduced volume expansion. The methods of synthesizing graphite and silicon composites include high energy mechanical milling [10], spray drying [11], chemical vapor deposition [12], and liquid solidification [13]. In a study by Jo and Lee [14], a phenol resin coated graphite/silicon composite afforded an initial discharge capacity of 495 mAh/g at 10 wt% Si, 89% capacity retention ratio, and 80% rate capability at 2 C/0.1 C. Lee and Lee [15] also reported that after the attachment of silica to surface-modified graphite and Mg thermal reduction, the pitch coated graphite/silicon composite has a high initial discharge capacity of 537 mAh/g at 28.5 wt% silica, as well

†To whom correspondence should be addressed.
E-mail: jdlee@chungbuk.ac.kr

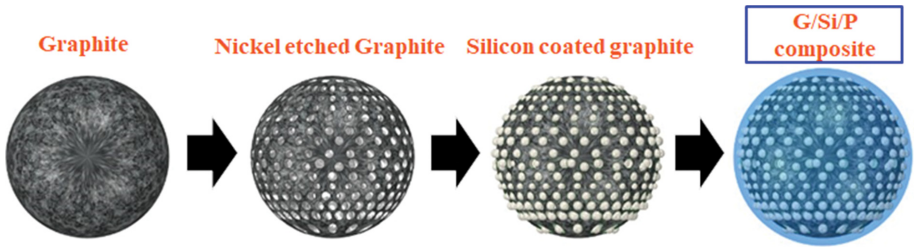

Fig. 1. Schematic diagram of the preparation process of graphite/silicon/pitch composites.

as excellent cycle stability, indicated by 95% capacity retention up to 30 cycles.

In this study, graphite/silicon/pitch composites as an anode material for LIBs are prepared and electrochemical properties of the composites are characterized. To prepare graphite/silicon/pitch composites, graphite was first etched by nickel metal to create spherical pores on the graphite surface, not only to reduce the diffusion distance of Li ions but also to insert silicon nanoparticle. The pore size was controlled depending on the calcination retention time and optimized for the insertion of silicon nanoparticles. Petroleum pitch was then coated onto graphite/silicon composites by using wet coating process to prepare the anode composites. The physical properties of the prepared graphite/silicon/pitch composites were investigated based on the ratio of each material by using scanning electron microscopy (SEM), X-ray diffraction (XRD), and thermal gravimetric analysis (TGA). Furthermore, the properties as an anode material for lithium secondary batteries were investigated by using the 1.0 M $LiPF_6$ (EC : DMC : EMC=1 : 1 : 1 vol%) electrolyte for electrochemical evaluation of the charge-discharge cycle, rate capability, cyclic voltammetry, and electrochemical impedance spectroscopy (EIS).

EXPERIMENTAL PROCEDURES

1. Preparation of Etched Graphite Using Nickel

Nickel chloride hexahydrate (SAMCHUN) was dissolved in distilled water, and graphite (MTI KOREA) was dispersed by ultrasonication. The resulting solution was dried in a vacuum oven at 120 °C to completely remove the moisture, and the sample was heat-treated under Ar gas for 20 min at 500 °C and for 1-3 h at 1,000 °C to form nano-sized nickel. After surface modification of graphite with nickel, the sample was stirred in HCl at 500 rpm for 8 h at room temperature for etching. Lastly, the sample was washed repeatedly until pH 7 was achieved, and after drying in a vacuum oven at 120 °C.

2. Attachment of Silicon to Etched Graphite

Silicon was surface-treated by stirring with APTES (Sigma Aldrich) in ethanol solvent, and attached to the graphite surface. The prepared graphite with spherical pores on the surface was dispersed in distilled water for 10 min, and silicon (Alfa Asear) was also dispersed in the solution, followed by stirring at 250 rpm for 24 h using a hotplate stirrer. After the distilled water was removed by drying in a 120 °C oven, the graphite/silicon composite was prepared.

3. Preparation of Graphite/Silicon/Pitch Composite

Petroleum pitch (SP 250 °C) was dispersed and dissolved in tetrahydrofuran (OCI Company, 99.5%) for 10 min using an ultrasonic cleaner. Following the addition of the prepared graphite/silicon sample, the sample was again treated with the ultrasonic cleaner for 30 min to achieve homogeneous dispersion. After stirring at 200 rpm for 24 h using the hotplate stirrer and drying, the pitch coated silicon/graphite composite was prepared. The resulting material was subjected to two-step calcination under Ar gas atmosphere for 30 min at 500 °C and for 1 h at 1,000 °C to prepare the pitch coated, artificial graphite. The final prepared graphite/silicon/pitch composites are denoted as $G_8Si_1P_1$ for the sample with a graphite : silicon : pitch composition ratio of (8 : 1 : 1), and $G_6Si_2P_2$ for (6 : 2 : 2) and $G_4Si_3P_3$ for (4 : 3 : 3). A schematic diagram of the process of preparing the graphite/silicon/pitch composite as an anode material for lithium ion batteries is presented in Fig. 1.

The surface properties of graphite/silicon/pitch composite materials were analyzed by SEM (Scanning Electron Microscope, (Ultra Plus, Zeiss, Oberkochen, Germany), XRD (X-ray diffraction, Bruker-D-5005, Billerica, MA, USA) and TGA (Thermogravimetric analysis, D-TGA, SDT 2960, TA Instruments, Champaign, IL, USA).

4. Electrochemical Measurements

The graphite/silicon/pitch anode composite was used as the active material to prepare the anode of secondary batteries, and Super-P was used as the conductive material, which was combined with CMC (carboxymethyl cellulose, MTI KOREA) and SBR (styrene-butadiene rubber, MTI KOREA). The coated electrode was dried in a 120 °C vacuum oven for 2 h, followed by compression using a roll press to fix the electrode density at 1.6±0.1 $g \cdot cm^3$. To analyze the electrochemical characteristics of the prepared electrode, a coin-type half-cell was produced using Li metal as the counter electrode in a glove box filled with Ar gas. The electrochemical analysis was carried out using a 25 μm thick trilayer separator membrane (Celgard 2400, Celgard, LLC, Charlotte, NC, USA) and a 2032 type coin cell. As the electrolyte, 1.0 M $LiPF_6$ (EC : DMC : EMC=1 : 1 : 1 vol%) was used.

RESULTS AND DISCUSSION

1. Physical Properties of the Graphite/Silicon/Pitch Composite

The field-emission scanning electron microscope (FE-SEM) images of nickel-etched graphite are presented in Fig. 2. It is evident that spherical pores were uniformly formed on the surface while maintaining the spherical shape of the artificial graphite. Nickel chloride hexahydrate was used for the formation of nickel on the graphite surface, and it was etched to a slightly more spherical shape than that using nickel acetate in the references [16]. The pore size was

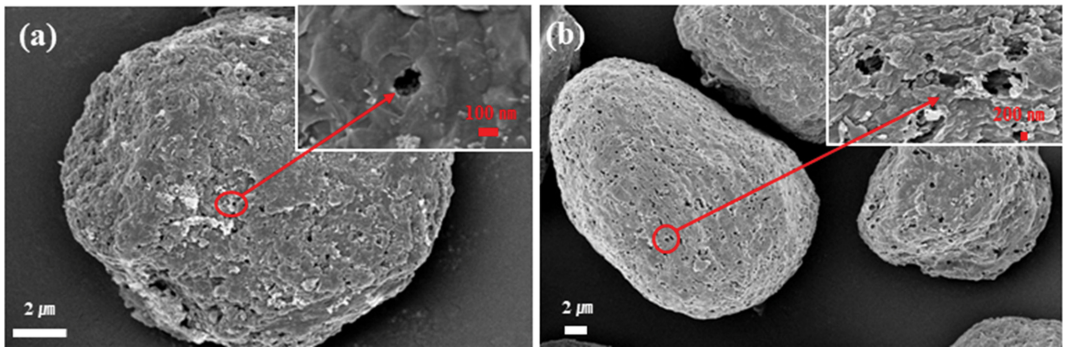

Fig. 2. SEM images of nickel etched graphite from different calcination time (a) 1 h and (b) 3 h.

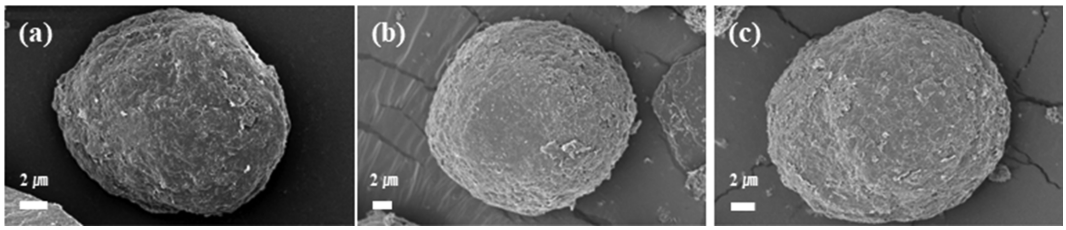

Fig. 3. SEM images of graphite/silicon/pitch composites (a) $G_8Si_1P_1$, (b) $G_6Si_2P_2$ and (c) $G_4Si_3P_3$.

controlled by regulating the calcination retention time during the process of nickel formation while heating at 500 °C. Retention for 1 h at 500 °C led to the formation of ~100 nm pores, while 3 h retention led to 700-800 nm pores. The specific surface area of nickel-etched graphite, which was 1.622 m^2/g, was increased compared to that of pristine graphite, which was 1.095 m^2/g. The increase of specific surface area is due to the nickel etching process creating many holes with large pore volume at the graphite surface [17].

Surface analysis of the graphite/silicon/pitch composite prepared by pitch coating after the insertion of silicon into the nickel-etched graphite pores is shown in Fig. 3. The pores that were formed by nickel etching completely disappeared in the prepared graphite/silicon/pitch composite, which is presumed to be due to silicon insertion and the pitch coating. Then, the spherical particle shape of the prepared composite was maintained.

XRD was used to determine the crystal structure of the prepared graphite/silicon/pitch composite, as presented in Fig. 4. For the graphite/silicon/pitch composite, the main peaks of graphite were detected at 26.4, 42.4, 44.4, 54.5, and 77.5°, in agreement with JCPDS Card No. 008-0415. The respective peaks correspond to the (002), (100), (101), (004), and (110) crystal planes, as in the previous study [18,19]. Diffraction peaks were also observed at 28.4, 47.3, 56.1, 69.1, and 76.3°, corresponding to the (111), (220), (311), (400), and (331) planes of silicon in JCPDS Card No. 77-2111 [20]. The pitch prepared after the carbonization process gave rise to a broad peak, indicating the amorphous morphology, as reported by Lee and Lee [7,15].

The TGA data for the graphite/silicon/pitch anode material are presented in Fig. 5. TGA was performed by ramping the temperature at 10 °C/min within the temperature range of 25-1,000 °C under

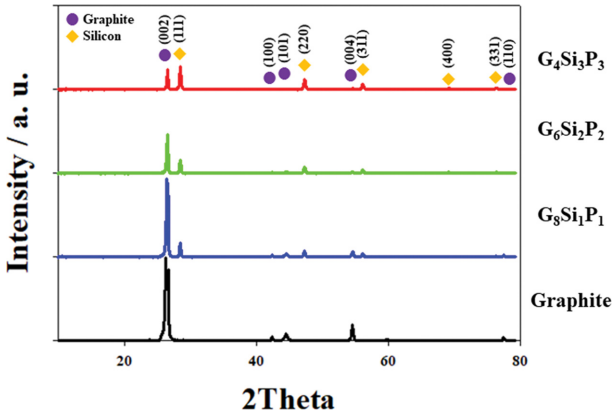

Fig. 4. XRD patterns of graphite/silicon/pitch composites.

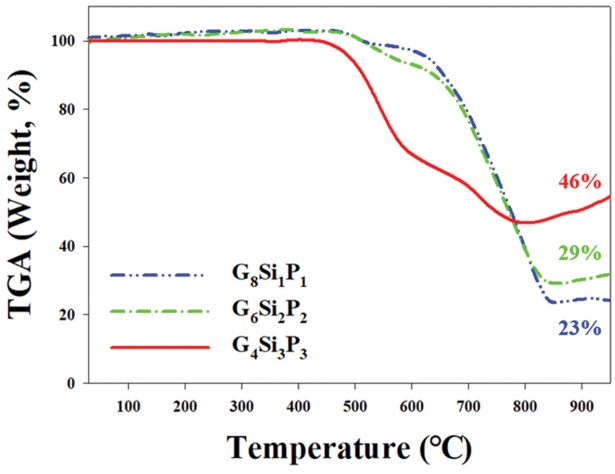

Fig. 5. TGA curves of graphite/silicon/pitch composites.

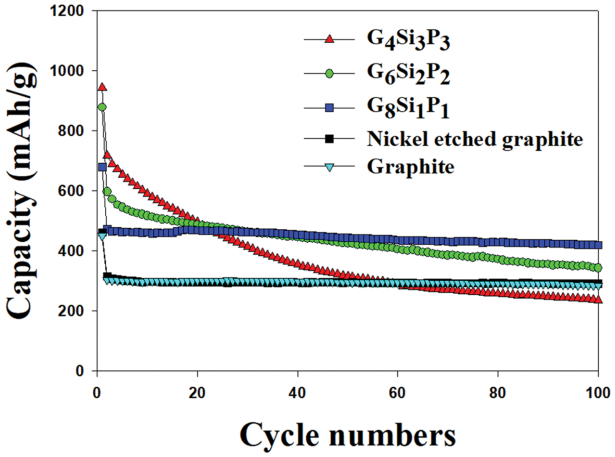

Fig. 6. Cycling performance of graphite/silicon/pitch composites.

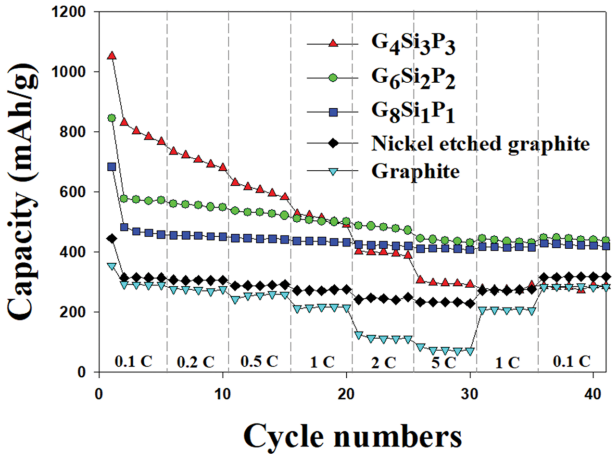

Fig. 7. Rate capability of graphite, nickel etched graphite and graphite/silicon/pitch composites.

air atmosphere. The TGA curve showed a 77% weight change for the $G_8Si_1P_1$ composite up to 500-750 °C due to the combustion of carbon after thermal decomposition with graphite; a 71% weight change was observed for the $G_6Si_2P_2$ composite and a 54% weight change for the $G_4Si_3P_3$ anode composite. An inflection point was detected in the TGA curve, which is thought to arise from the composite containing two carbon materials: graphite and pitch carbon [21]. The rise in the TGA curve after approximately 830 °C is presumed to be due to silicon oxidation [22].

2. Electrochemical Characteristics of Graphite/Silicon/Pitch Composite

To evaluate the electrochemical performance of the graphite/silicon/pitch composites ($G_8Si_1P_1$, $G_6Si_2P_2$, and $G_4Si_3P_3$) based on the composition of each material, cycle tests were performed. Fig. 6 presents the charge-discharge cycle test data obtained at 0.1 C. The initial reversible capacity was 451, 461, 680, 878, and 943 mAh/g for graphite, nickel-etched graphite, $G_8Si_1P_1$, $G_6Si_2P_2$, and $G_4Si_3P_3$, respectively. The data show that the capacity of nickel-etched graphite increased more than that of graphite due to the increase of the specific surface area, while the initial discharge capacity of graphite/silicon/pitch composites increased with the silicon content. The initial Coulombic efficiency was 79, 90, 64, 70, and 71% for graphite, nickel-etched graphite, $G_8Si_1P_1$, $G_6Si_2P_2$, and $G_4Si_3P_3$, respectively. Compared to that of graphite without surface treatment, the initial efficiency of nickel-etched graphite increased up to 90%, but rapidly decreased after the addition of silicon. Also, initial efficiency of the graphite/silicon/pitch composite increased with increasing pitch content. The capacity retention of the composite anode material was evaluated with 94, 92, 90, 60, and 34%, respectively, after 100 cycles. Thus, for up to 10 wt% silicon content, a high capacity retention rate was maintained for 100 cycles, but graphite/silicon/pitch composites with a high silicon content showed a rapidly decreasing rate.

Rate capability of the anode composites was evaluated at various C-rate from 0.1 to 5 C and the result is illustrated in Fig. 7. The rate of capacity retention for nickel-etched graphite was 74% at 5 C/0.1 C, indicating an improvement in the rate capability compared with graphite. Nickel-etched graphite is thought to have an enhanced capacity compared to pristine graphite due to its porous structure. The pores at the surface not only increased the number of sites for Li ions to intercalate and de-intercalate, which facilitated the charge and discharge speeds at a high C-rate, but also reduced the diffusion distance of Li ions [23]. The capacity retention ratio for $G_8Si_1P_1$ was 91% at 2 C/0.1 C and 87% at 5 C/0.1 C. And the capacity recovery rate at 0.1 C/0.1 C was 92%, corresponding to the most outstanding capacity characteristics. In contrast, the $G_4Si_3P_3$ composite delivers a relatively poor rate capability, as the silicon content increases.

Cyclic voltammetry (CV) was used to examine the electrochemical reaction at the electrode interface. Fig. 8 shows the CV results by using a coin cell prepared with the graphite/silicon/pitch composite, for five cycles at 0.1 mV/s scan rate. In the first cycle, a broad reduction peak due to the formation of an SEI layer was observed between 0.3 and 0.8 V, while the peak was no longer observed in the second or any subsequent cycle. This implies a significant improvement in the reversibility of the insertion-extraction of lithium ions. In addition, a reduction peak due to the insertion of lithium ions was detected at around 0.15 V, whereas at ~0.2 V and 0.45 V, an oxidation peak due to the extraction of lithium ions was detected [24]. These peaks are thought to arise from lithium-ion insertion and extraction among the graphite layers at <0.2 V during the charge-discharge process, whereas in the silicon alloy, lithium-ion insertion occurred at approximately 0.2 V and dealloying occurred mainly at 0.45 V [25,26].

Electrochemical impedance spectroscopy (EIS) is suitable for measuring the rate of Li^+ diffusion and electrical conductivity. The EIS curve profile of the anode material prepared in this study showed a semi-circle in the high-frequency domain and a linear slope in the low-frequency domain [27]. As shown in Fig. 9(b), the electrolyte resistance (Re) indicates conductivity at the initial stage of the Nyquist plot [23,28]. The Re of the pristine graphite is 1.6 Ω, which is the lowest among other materials. As shown in Fig. 9(a), the charge transfer resistance (Rct) can be confirmed by the diameter of the semicircle. The etched graphite has a smaller semicircle size than the graphite because the increased number of active sites improved the electrochemical reaction [23]. Also, the semicircle was

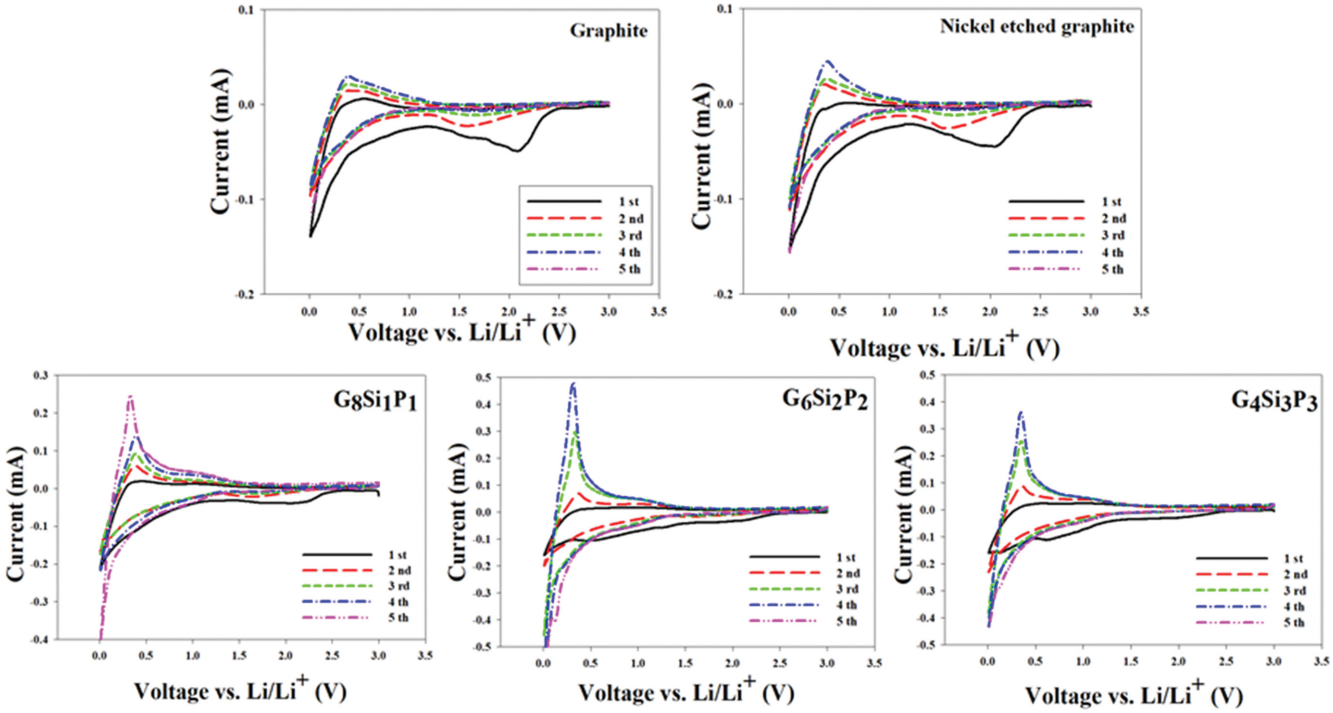

Fig. 8. Cyclic voltammograms of graphite/silicon/pitch composites.

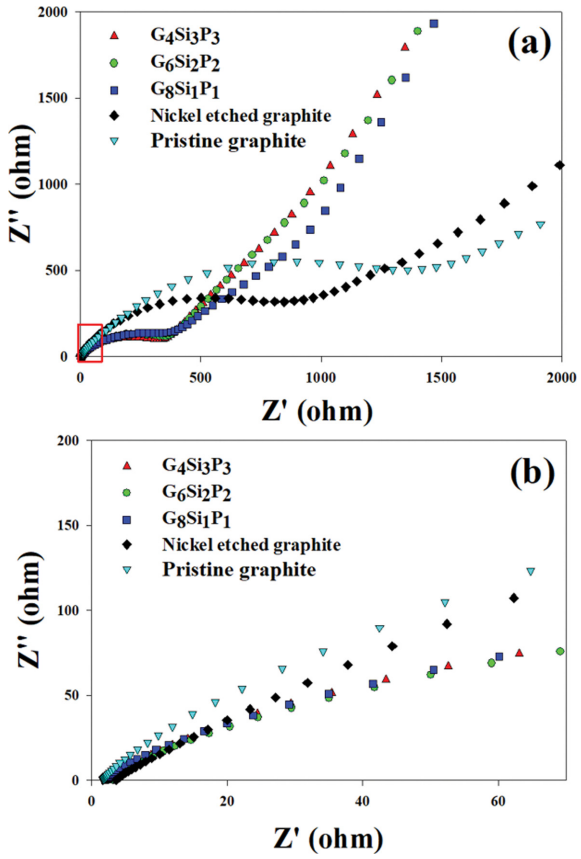

Fig. 9. Impedence spectra of graphite/silicon/pitch composites (a) Nyquist plot and (b) the amplification of the square part in (a).

the smallest in case of the graphite/silicon/pitch composite material due to the addition of silicon [28]. The resistance of the composite materials sequentially declined in the following order: $G_8Si_1P_1$, $G_6Si_2P_2$, $G_8Si_1P_1$.

CONCLUSION

A pitch coated graphite/silicon composite using nickel etching process was synthesized to improve the capacity and rate performance of the anode material. Etched graphite with 100-800 nm pore size was prepared, and then the pitch coated graphite/silicon composite was synthesized using wet processing. The electrochemical properties of the anode material were investigated according to the composition ratio of graphite, silicon, and pitch. Nickel-etched Graphite has an initial reversible capacity of 461 mAh/g with an initial efficiency of 90%, which is superior to that of graphite. The $G_8Si_1P_1$ (graphite : silicon : pitch=8 : 1 : 1) composite material showed an initial reversible capacity of 680 mAh/g, a capacity retention ratio of 90%, and a retention rate of 87% at 5 C/0.1 C. This is the result showing the best electrochemical properties among the prepared anode materials. Therefore, it was confirmed that the pitch coated graphite/silicon composite could be used as an anode material for a high-performance lithium ion battery that replaces the commercialized graphite.

ACKNOWLEDGEMENTS

This research was supported by Korea Evaluation Institute of Industrial Technology (KEIT) through the Carbon Cluster Construction project [10083621, Development of preparation technology

in petroleum-based artificial graphite anode] funded by the Ministry of Trade, Industry & Energy (MOTIE, Korea).

REFERENCES

1. M. Li, J. Lu, Z. Chen and K. Amine, *Adv Mater.*, **30**, 1800561 (2018).
2. Z. P. Cano, D. Banham and S. Ye, *Nat Energy*, **3**(4), 279 (2018).
3. Y. J. Jo and J. D. Lee, *Korean Chem. Eng. Res.*, **57**(1), 5 (2019).
4. N. Kim, S. Chae, J. Ma, M. Ko and J. Cho, *Nat. Commun.*, **8**, 1 (2017).
5. P. Li, J. Y. Hwang and Y. K. Sun, *ACS NANO*, **13**, 2624 (2019).
6. J. Nzabahimana, P. Chang and X. Hu, *J. Mater. Sci.*, **51**, 4798 (2019).
7. S. Y. Lee and J. D. Lee, *Korean Chem. Eng. Res.*, **56**(4), 561 (2018).
8. G. Y. Gor, J. Cannarella, J. H. Prévost and C. B. Arnold, *J. Electrochem. Soc.*, **161**, 3065 (2014).
9. Y. J. Jo and J. D. Lee, *Korean J. Chem. Eng.*, **36**(10), 1724 (2019).
10. Y. S. Yoon, S. H. Jee, S. H. Lee and S. C. Nam, *Surf. Coat. Technol.*, **206**, 553 (2011).
11. Z. Wang, Z. Mao, L. Lai, M. Okubo, Y. Song, Y. Zhou, X. Liu and W. Huang, *Chem. Eng. J.*, **313**, 187 (2017).
12. M. Ko, S. Chae, J. Ma, N. Kim, H. W. Lee, Y. Cui and J. Cho, *Nat. Energy*, **1**, 16113 (2016).
13. S. Y. Kim, J. Lee, B. H. Kim, Y. J. Kim, K. S. Yang and M. S. Park, *ACS Appl. Mater. Interfaces*, **8**, 12109 (2016).
14. Y. J. Jo and J. D. Lee, *Korean Chem. Eng. Res.*, **56**(3), 320 (2018).
15. S. H. Lee and J. D. Lee, *Korean Chem. Eng. Res.*, **57**(1), 118 (2019).
16. H. Cao, X. Zhou, C. Zheng and Z. Liu, *Carbon*, **89**, 41 (2015).
17. J. Kim, S. M. N. Jeghan and G. Lee, *Micropor. Mesopor. Mater.*, **305**, 110325 (2020).
18. J. H. Lee, W. J. Kim, J. Y. Kim, S. H. Lim and S. M. Lee, *J. Power Sources*, **176**, 353 (2008).
19. J. Lai, H. Guo, Z. Wang, X. Li, X. Zhang, F. Wu and P. Yue, *J. Alloys Compd.*, **530**, 30 (2012).
20. M. Z. Jung, J. Y. Park and J. D. Lee, *Korean Chem. Eng. Res.*, **54**(1), 16 (2016).
21. I. T. Kim, J. Lee, J. C. An, E. Jung, H. K. Lee, M. Morita and J. Shim, *Int. J. Electrochem. Sci.*, **11**, 5807 (2016).
22. H. S. Ko, J. E. Choi and J. D. Lee, *Appl. Chem. Eng.*, **25**, 592 (2014).
23. Q. Cheng, R. Yuge, K. Nakahara, N. Tamura and S. Miyamoto, *J. Power Sources*, **284**, 258 (2015).
24. N. L. Rock and P. N. Kumta, *J. Power Sources*, **164**, 829 (2007).
25. L. Gan, H. Guo, Z. Wang, X. Li, W. Peng, J. Wang, S. Huang and M. Su, *Electrochim. Acta*, **104**, 117 (2013).
26. M. J. Jung and J. D. Lee, *Appl. Chem. Eng.*, **26**, 80 (2016).
27. J. Xie, L. Tong, L. Su, Y. Xu, L. Wang and Y. Wang, *J. Power Sources*, **342**, 529 (2017).
28. J. J. Wu and W. R. Bennett, *2012 IEEE Energytech*, IEEE (2012).